Preferential use of unobstructed lateral portals as the access route to the pore of human ATP-gated ion channels (P2X receptors)

Damien S K Samways, Baljit S Khakh, Sébastien Dutertre, Terrance M Egan

Preferential use of unobstructed lateral portals as the access route to the pore of human ATP-gated ion channels (P2X receptors)

Damien S. K. Samways[a], Baljit S. Khakh[b], Sébastien Dutertre[c], and Terrance M. Egan[a,1]

[a]Department of Pharmacological and Physiological Science, and The Center for Excellence in Neuroscience, Saint Louis University School of Medicine, St. Louis, MO 63104; [b]Departments of Physiology and Neurobiology, David Geffen School of Medicine, University of California, Los Angeles, CA 90095; and [c]Institute for Molecular Bioscience, University of Queensland, St. Lucia, QLD 4067, Australia

Edited* by Michael V. L. Bennett, Albert Einstein College of Medicine, Bronx, NY, and approved July 12, 2011 (received for review November 29, 2010)

P2X receptors are trimeric cation channels with widespread roles in health and disease. The recent crystal structure of a P2X4 receptor provides a 3D view of their topology and architecture. A key unresolved issue is how ions gain access to the pore, because the structure reveals two different pathways within the extracellular domain. One of these is the central pathway spanning the entire length of the extracellular domain and covering a distance of ≈70 Å. The second consists of three lateral portals, adjacent to the membrane and connected to the transmembrane pore by short tunnels. Here, we demonstrate the preferential use of the lateral portals. Owing to their favorable diameters and equivalent spacing, the lateral portals split the task of ion supply threefold and minimize an ion's diffusive path before it succumbs to transmembrane electrochemical gradients.

fenestration | fractional calcium current | ligand-gated ion channel | cysteine scanning mutagenesis

P2X receptors are a family of ligand-gated ion channels that open when bound to extracellular ATP, providing a regulated path for depolarizing cation current across cell surface membranes. In mammals, the resulting entry of Ca^{2+} and Na^{+} triggers muscle contraction, release of neurotransmitters, hormones, and inflammatory mediators, as well as activation of downstream signaling cascades (1, 2). In combination with a ubiquitous distribution, the widespread actions of ATP suggest that P2X receptors play essential roles in the body. Indeed, advances with mouse genetics and pharmacology show that P2X receptors are involved in a variety of important physiological responses and disease states (3), making them attractive targets for drug discovery. A key goal is to understand how P2X receptors work at a molecular level.

The P2X receptor family is made of seven gene products, designated P2X1–P2X7, that can form homomeric and/or heteromeric assemblies (4). One family member, the PX4 receptor, is particularly prevalent in the central nervous system (5). This receptor is involved in microglia–neuron interactions, and mounting evidence suggests it plays a critical role in neuropathic pain, a persistent and prevalent form of pain whose molecular and cellular neurobiology is poorly understood and for which there is no effective treatment (6).

Each P2X4 receptor is made of three parts: an extracellular domain containing the ATP binding site and the extracellular vestibule of the ion channel, a transmembrane pore containing the channel gate and selectivity filter, and an intracellular vestibule in contact with the cytoplasm (7). The possibility that the permeation pathway extends outward from the extracellular vestibule was not considered until recently, when the newly solved crystal structure of a closed state of the zebrafish P2X4.1 receptor (zfP2X4.1R) revealed, but failed to discriminate between, two possible paths in the extracellular domain for ion passage to the pore (8). The first is the central pathway that spans the entire length of the extracellular domain (Fig. 1*A*). The central pathway is lined with negative charge and appears well suited to regulate cationic current (8, 9). The second pathway is cast from three lateral portals formed at the interfaces of adjoining subunits just above the outer leaflet of the membrane (Fig. 1*B*). The lateral portals are less charged than the central pathway, and less obstructed. Dual pathways are also observed in acid sensing channels (10), but in neither case is it known which pathway is functionally used as a cation pore.

Early work showed that replacing Ile^{328} of the rat P2X2 receptor (rP2X2R) with cysteine results in a mutant receptor whose ATP-gated currents are sensitive to water-soluble, thiol-reactive reagents (11, 12), and a recent report used the P2X2R-I328C mutant to conclude that the lateral portals form an access route to the transmembrane pore (13). However, Ile^{328} sits at the top of the second transmembrane domain of the rP2X2R and is accessible to thiol-reactive reagents that may travel through either the central pathway or the lateral portals and, thus, this mutant does not firmly establish the primary route of ion flow. In the present report, we used whole-cell as well as single-channel recordings, and applied cationic and anionic methanethiosulfonates (MTS) and Cd^{2+} in the presence and absence of ATP, to measure effects on gating and conduction of a wide range of cysteine-substituted mutants of the human P2X4 receptor (hP2X4R). Taken together, our experiments provide convincing evidence that the lateral portals form the primary access route to the hP2X4R and show that some residues in the lateral portals are subject to allosteric modulation.

Results

We used cysteine-scanning mutagenesis (14) and measurements of fractional Ca^{2+} current ($Pf\%$) (15, 16) to investigate the contributions of the two pathways to ionic current of the hP2X4R. We studied the hP2X4R because of its high sequence identity to the zfP2X4.1 form (Fig. S1) and, because, unlike the zfP2X4.1R (17), it readily expresses in HEK293 cells and gives reproducible responses to repeated applications of micromolar concentrations of ATP (EC_{50} = 4.4 ± 0.9 μM; n = 6; Fig. 2*A*). Using a homology model of the hP2X4R closed state, we identified residues that line the central pathway and the lateral portals in their narrowest regions and, thus, might be expected to interact with ions in the two putative permeation pathways. We then mutated the residues to cysteines, expressed the mutants in HEK293 cells, and measured the accessibility of the engineered thiol side chains to water-soluble methanethiosulfonates (MTS) by means of electrophysiology (*SI Methods*). In control experiments, we found no effect of 1 mM [2-(trimethylammonium) ethyl] MTS^{+} ($MTSET^{+}$) on the ATP-gated (100 μM) current of the wild-type (*wt*) hP2X4R (Fig. 2 *B* and *C*).

To demonstrate feasibility, we used the published reports of accessibility of cysteine-substituted rP2X2Rs (11, 12, 18, 19) to suggest a residue in the transmembrane pore of hP2X4R (Ser^{341}, equivalent to rP2X2R-T336C) that should be accessible to $MTSET^{+}$ (Fig. S2*A*). As expected, we found that 1 mM $MTSET^{+}$ irreversible reduced (99 ± 1%, n = 4) the agonist-gated current of

Author contributions: D.S.K.S., B.S.K., S.D., and T.M.E. designed research, performed research, analyzed data, and wrote the paper.

The authors declare no conflict of interest.

*This Direct Submission article had a prearranged editor.

[1]To whom correspondence should be addressed. E-mail: egantm@slu.edu.

This article contains supporting information online at www.pnas.org/lookup/suppl/doi:10.1073/pnas.1017550108/-/DCSupplemental.

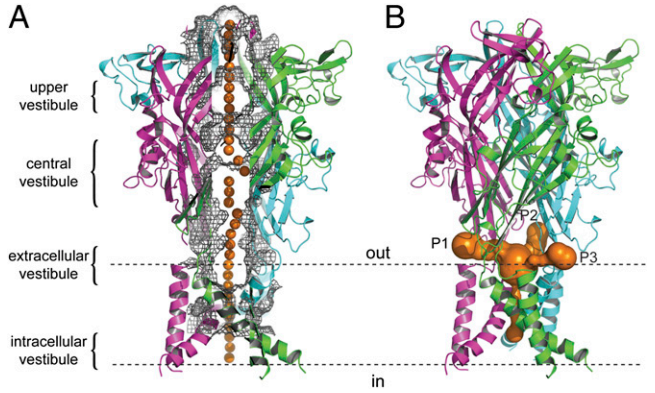

Fig. 1. Alternative ion access routes to the pore of the hP2X4R. Illustrations of the hP2X4R viewed parallel to the membrane plane. The cytoplasmic N- and C-termini are missing because these domains are absent in the crystal structure of the truncated zfP2X4.1 (8). The dotted lines show the limits of the membrane. (*A*) A sagittal section (4 Å) of the central pathway shows the pore-lining inner surface (gray mesh grid), highlighting the vestibules and constrictions defined by Kawate et al. (8). The orange spheres are spaced in 1-Å steps along the long axis of the pore and suggest a likely path for cations to the cytoplasm if they entered through the central pathway (calculated by using PoreWalker 1.0). (*B*) A space-filling model of the lateral portals, extracellular vestibule, and transmembrane pore (orange) as calculated by using CAVER. Each portal (P1 to P3) has a wide (8 Å) and direct opening to the extracellular vestibule of the transmembrane pore.

the hP2X4R-S341C when coapplied with ATP (Fig. S2 *B* and *E*), and that the rate of modification (K_{on} = 4,387 ± 1,472 $M^{-1}{\cdot}s^{-1}$) was comparable to that measured when $MTSET^+$ and ATP are coapplied to cysteine-substituted rP2X2R (18). Because the large (6 × 6 × 10 Å) $MTSET^+$ must first traverse either the central pathway or the lateral portals to reach S341C, this experiment serves as a positive control to demonstrate that the relevant permeation pathway is fully permeable to the thiol-modifying reagent.

Upper Vestibule. We examined the central pathway by placing cysteines at sites in the upper vestibule where the diameter of the channel is narrow (Fig. 2*D*). The first site represents the outermost entrance to the central pathway; it is obstructed in the closed state model of hP2X4R, in part because the side chain of Leu^{303} caps the opening. The entrance must open for current to flow, and we hypothesized that modification by $MTSET^+$ of L303C would plug the open channel and reduce ATP-gated current if the central pathway formed a conducting pore. However, we saw no effect of coapplying ATP and $MTSET^+$ on L303C currents (Fig. 2*D*), and no effect of $MTSET^+$ on the neighboring D302C and A304C residues (<5% change; n = 5). We then moved inward, and placed cysteines near the top (A297C; pore diameter ≈ 10 Å) and bottom (P92C and N93C; pore diameter ≈ 5 Å; Fig. S3) of the upper vestibule, and again saw no effect (<5% change; n = 5) of $MTSET^+$ (for examples, see Fig. 2*D*). The bulkier (≈8 × 16 × 16 Å) Texas Red-2-sulfonamidoethyl MTS (MTSTR) was also without effect at all of the aforementioned residues, despite the fact that it irreversibly blocks the current of the S341C transmembrane mutant (Fig. S2 *C* and *E*).

Next, we probed the narrow constriction (≈2.3 Å) between the upper and central vestibules of the zfP2X4.1R formed in part by three residues (Gln^{97}, Glu^{98}, Asp^{99}), including Glu^{98} that coordinates Gd^{3+} just above the entrance to the central vestibule (8). We placed cysteines at the equivalent sites of the hP2 X 4R (Gln^{94}, Glu^{95}, Glu^{96}; Fig. S3) and failed to measure an effect of $MTSET^+$ (Fig. 2 *D* and *E*) or MTSTR. Although it is possible that $MTSET^+$ and MTSTR modify residues in the constriction without changing current amplitude (14), the comparative dimensions of the MTS head groups and the diameter of the pathway (8) render this highly unlikely. Another possibility is that residues in the constriction are inaccessible to $MTSET^+$ and MTSTR, either because the central pathway does not form a part of the ion channel pore, or because large MTS reagents are impermeable. Although the latter option seems unlikely because of the demonstrated accessibility of the downstream S341C mutant, we nevertheless tested this possibility by using Cd^{2+}, a small metal element that binds to thiol side chains exposed to water, as a permeable probe (19). We expected to measure a change in the amplitude of the ATP-gated current if the coordinated ion occludes the channel or preferentially locks it in the open or closed state, but we found that Cd^{2+} (20 μM) failed to modify (<5% change; n = 6–7) the ATP-evoked currents of any of these three hP2X4R mutants. When considered in concert with the A93C/A297C/L303C experiments, our results argue against the suggestion that the central pathway forms a major conduit for ion conduction in the hP2X4R (8, 9).

Lateral Portals. We then tested the alternative hypothesis that cations enter the transmembrane pore through the lateral portals. We started by studying two acidic residues in the lateral portals of the hP2X4R, Glu^{56} and Asp^{58} (Fig. 3*A*), that are common to most (P2X2-P2X7) but not all (P2X1) human P2X receptors, and that are thought to concentrate cations in the extracellular vestibule of the zfP2X4.1R pore (8). Fig. 3 shows the effect of coapplying $MTSET^+$ and ATP. The results were qualitatively similar in both mutants: $MTSET^+$ caused irreversible reductions in the amplitudes of the ATP-gated currents. In cells expressing the E56C mutant, $MTSET^+$ reduced current by 58 ± 4% (n = 9), with an apparent modification rate (K_{on}) of 7,057 ± 421 $M^{-1}{\cdot}s^{-1}$ (Fig. 3*B*). By comparison, $MTSET^+$ caused a slower (K_{on} = 3,545 ± 577 $M^{-1}{\cdot}s^{-1}$) but more complete block (95 ± 1%, n = 8) of the D58C mutant (Fig. 3*C*). The faster block of E56C may reflect the fact that the substituted cysteine resides on the outer surface of the portal where it is more accessible to $MTSET^+$ than D58C (Fig. S3).

Although Glu^{56} and Asp^{58} are positioned in the lateral portals/extracellular vestibule, they also lie at the lowest point of the central pathway. Therefore, it remained possible that the $MTSET^+$-sensitive currents move through the central pathway before reacting with the engineered thiolates. We addressed this possibility.

First, we measured $MTSET^+$ reactivity in the absence of ATP. The central pathway contains several narrow constrictions that must open to allow $MTSET^+$ to access Glu^{56} and Asp^{58} (8). In contrast, there is no barrier to current flow in the portals that would prevent modification of the closed states of E56C and D58C mutants. We established baseline responses to ATP (100 μM), and then applied $MTSET^+$ for 2–60 s in the absence of ATP. In all cases, $MTSET^+$ caused significant and persistent inhibitions of currents elicited by subsequent applications of ATP (Fig. 3 *D* and *E*). In some cases, the ATP-gated currents showed a partial recovery in the first 3 min after washout of $MTSET^+$. A similar effect is reported for $MTSET^+$ inhibition of cysteine-substituted rat P2X4Rs, which is thought to reflect recycling of unmodified receptors to the plasma membrane (20) (see also ref. 7). However, in no case did the amplitude of the ATP currents return to their control values, and a significant inhibition remained even after a 15-min wash (Fig. 3 *D*–*F*). Further, the persistent inhibition of ATP-gated current by $MTSET^+$ was immediately and fully reversed by the reducing agent, DTT (1 mM; 60 s) (Fig. 3 *D*–*F*). The same protocol had no effect on the *wt* hP2X4R (Fig. 2*C*), or on mutant receptors containing cysteine substitutions in the narrowest constriction of the central pathway (Fig. 2*E*), suggesting that the majority of the plasmalemmal E56C and D58C receptors were covalently modified by $MTSET^+$.

Second, we measured the ability of an anionic MTS reagent to modify E56C and D58C. The profoundly acidic surface of the central vestibule of the zfP2X4.1R provides a long-range negative electrostatic environment that favors the passage of cations over anions (8, 13). The hP2X4R shows a modest Cl^- permeability (21), and we find that the anionic thiol-reactive drug, (2-sulfonatoethyl) MTS^- ($MTSES^-$), causes a fast (8,348 ± 867 $M^{-1}{\cdot}s^{-1}$) and near complete block of the S341C mutant (Fig. S2 *D* and *E*), as previously shown for the homologous residue (Thr^{336}) of the rP2X2R (11). Like $MTSET^+$, $MTSES^-$ must pass through either the central pathway or the lateral portals before reaching S341C. Therefore,

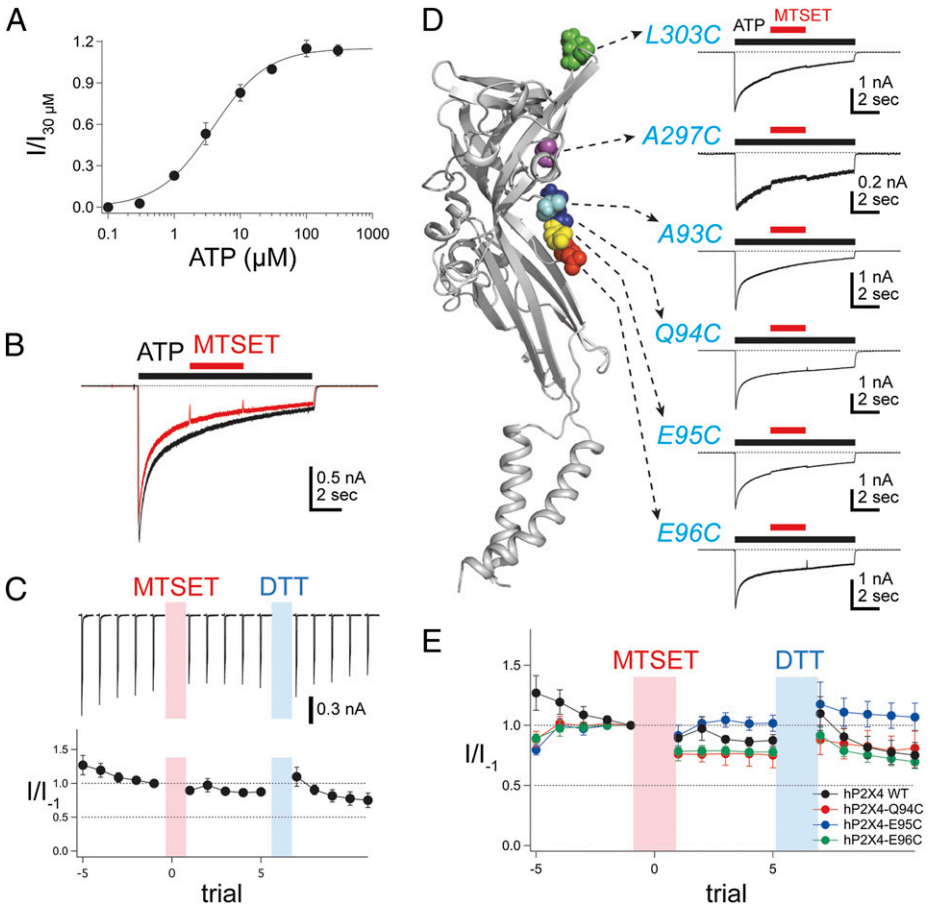

Fig. 2. MTSET$^+$ has no effect on *wt* hP2X4R and upper vestibule mutants. (*A*) Concentration–response curve for the hP2X4R generated by using perforated-patch electrophysiology (*SI Methods*). In each cell, 30 μM ATP was applied first, and then the effect of subsequent doses were normalized to the current caused by 30 μM ATP ($I/I_{30\mu M}$, *y* axis). (*B*) Sequential overlaid traces of ATP-gated current, separated by 180s, are shown before (black) and during (red) an application of MTSET$^+$. MTSET$^+$ (1 mM; red bar) has no effect on membrane current of the *wt* hP2X4R when coapplied with ATP (100 μM; black bar). (*C*) MTSET$^+$ (1 mM) has no effect on the *wt* hP2X4R when applied in the absence of ATP. *C Upper* shows the ATP-gated currents caused by repeated applications (each 1-s application is separated by 180s) before and after a 60 s application of 1 mM MTSET$^+$ (pink shaded rectangle). A subsequent application of DTT (1 mM, 60 s; blue shaded rectangle) also had no effect on the ATP-gated currents. *C Lower* shows the averaged data of individual measurements from five or more cells. Peak amplitudes of ATP-gated currents were normalized to the peak current of the ATP-gated current that immediately preceded the application of MTSET$^+$ (trial$_{-1}$). (*D*) Coapplied MTSET$^+$ has no effect on cysteine-substituted mutants of the central pathway. The illustration shows one subunit of the trimeric hP2X4R. The positions of six of the nine substituted cysteines in the central pathway are shown as spheres, and the traces at *Right* show the lack of effect of MTSET$^+$ (red bars) on currents evoked by ATP (black bars). (*E*) MTSET$^+$ (1 mM) and DTT (1 mM) have no effect on mutants of the narrow constriction of the central pathway when applied in the absence of ATP. Each data point is the average of individual determinations from seven or more cells measured using perforated-patch electrophysiology.

we coapplied MTSES$^-$ (1 mM) and ATP (100 μM) to measure accessibility and found that it modified both E56C and D58C mutant receptors. MTSES$^-$ caused a small (34%) but significant ($P = 0.0003$) potentiation of current through hP2X4R-E56C and a near complete block of ATP-gated current through hP2X4-D58C (Fig. S4 *A–C*). In cysteine substituted accessibility experiments, potentiation and block are both equally insightful and interpreted to indicate side chain accessibility (14). Surprisingly, the apparent modification rate at position D58C was faster for MTSES$^-$ (K_{on} = 10,681 ± 1,123 $M^{-1}{\cdot}s^{-1}$, $n = 7$) than for MTSET$^+$ (≈3,500 $M^{-1}{\cdot}s^{-1}$). We do not know why the anionic drug reacts quicker. Nonetheless, the fast reaction rate suggests that MTSES$^-$ has an unimpeded route of access to the thiol side chain of D58C, a situation that favors the short and less charged environment of the lateral portals over the longer and highly electronegative central pathway.

Finally, we measured the effect of MTSET$^+$ and MTSES$^-$ on T57C because it sits between the two acidic amino acids of the lateral portals. Coapplication of MTSET$^+$ caused a moderate (27 ± 5%; $n = 5$) but significant ($P = 0.0004$) inhibition of the ATP-gated current of hP2X4R-T57C (Fig. S4*D*). In contrast, MTSES$^-$ had no affect. However, an initial application of MTSES$^-$ prevented the inhibition of ATP-gated current by a subsequent application of MTSET$^+$ (Fig. S4*E*), showing that the anionic reagent modifies the cysteine at position Tyr[57].

Studies of Single Channel Current. The block of the ATP-gated currents of hP2X4R-E56C and hP2X4-D58C by MTSET$^+$ reflects either a change in conductance or a change in gating (14). Although both effects signal accessibility, a change in conductance is the more direct demonstration that the modified side-chain lines the permeation pathway (14, 22, 23). To measure a change in conductance, we recorded ATP-gated single channel currents from the membrane patches of HEK293 cells voltage-clamped at −120 mV. The hP2X4R shows a fast and progressive loss of single channel activity in excised patches that severely limits before and after comparisons of drug effects (24). Rundown also occurs in cell-attached patches, but at a slower rate that allows repeated measurements of single channel current amplitude (Fig. S5*A*; ref. 24). Thus, we used the cell-attached mode to compare channel amplitudes from populations of cells bathed in a physiological salt solution with or without 1 mM MTSET$^+$ before seal formation (*SI Methods*).

We recorded bursts of single-channel current from *wt* (Fig. S5*B*) and mutant hP2X4Rs (Fig. 4*A*) in the presence of ATP (0.3–1 μM) that were never seen in the absence of agonist or in untransfected cells. We found no difference in the conductances of the *wt* hP2X4R and the E56C single channel currents that measured 17.8 ± 0.8 pS ($n = 7$) and 16.2 ± 0.4 pS ($n = 23$), respectively. In contrast, the conductance of the D58C mutant (21.7 ± 0.6, $n = 26$) was significantly larger than that of the other two ($P < 0.01$), providing the first clue that D58C lines the permeation pathway. We then compared the average current amplitudes of the two cysteine-substituted receptors expressed in HEK293 cells bathed for 3 min in 1 mM MTSET$^+$ and saw significant ($P < 0.0001$) reductions (≈15% for E56C and ≈40% for D58C) in the size of the single channel currents (Fig. 4*B*). The fact that cysteine modification decreases conductance provides robust support for the model that E56C and D58C line the permeation pathway and, thus, validates the hypothesis that the lateral portals are a primary entrance to the transmembrane pore.

The ATP-gated whole-cell current of the hP2X4R-E56C is potentiated by coapplication of MTSES$^-$ (Fig. S4*A*). To determine whether this potentiation reflects a change in conduction or gating, we measured single channel current after anionic thi-

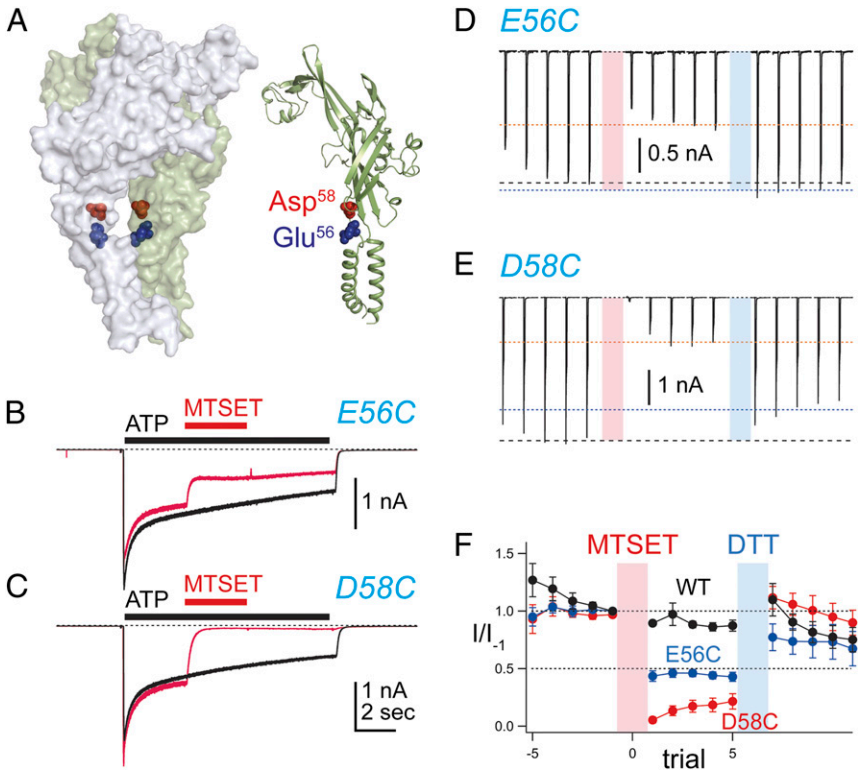

Fig. 3. MTSET$^+$ modifies residues of the lateral portals. (*A*) Illustrations of hP2X4R showing the position of Glu^{56} (blue spheres) and Asp^{58} (red spheres) in the lateral portals. (*B*) MTSET$^+$ (1 mM; red bars) inhibited current through hP2X4R-E56C when coapplied with ATP (100 μM; black bars). (*C*) MTSET$^+$ (1 mM) caused a near complete inhibition of current through hP2X4R-D58C when coapplied with ATP (100 μM). (*D* and *E*) MTSET$^+$ (1 mM for 60 s; pink shade rectangles) also inhibited current when applied in the absence of ATP. The inhibitions by MTSET$^+$ were reversed by 1 mM DTT (blue shaded rectangles). (*F*) Averaged data for experiments like those of *D* and *E*. Each data point is the average of individual measurements from 11 to 16 cells obtained by using perforated-patch electrophysiology.

olation and found a significant ($P < 0.0001$) increase (≈24%) in the size of the single channel current compared with control (Fig. 4 *A* and *B*). The observation that MTSET$^+$ and MTSES$^-$ have opposite effects suggests a role for electrostatics in the effect of thiolation on ATP-gated current at this position in the lateral portals.

No Effect of Removing the Fixed Negative Charge of Glu^{56}, Asp^{58}, and Glu^{95} on Ca^{2+} Current. In light of the apparent role of electrostatics described above, we next tested the hypothesis put forth by Kawate et al. that the fixed negative charge of Glu^{56} and Asp^{58} creates a long-range electrostatic potential that concentrates cations and repels anions near the entrance to the transmembrane pore (8). Ca^{2+} carries twice the charge of Na^+ and is more sensitive to local changes in electrostatic fields. Thus, we measured the fraction of the total ATP-gated current carried by Ca^{2+}, called the *Pf*%, by using patch clamp photometry as described (21, 25). We constructed single (E56Q, D58N) and double (E56Q/D58N) hP2X4R mutants with reduced charge and found that the *Pf*% was unchanged (Fig. S6). We therefore conclude that neither Glu^{56} nor Asp^{58} make a significant contribution to cation or anion selection in the hP2X4R, despite the fact that they lie in the permeation pathway. This result is consistent with the fact that the negative charges at these positions are not absolutely conserved among cationic P2X receptors. In a similar vein, we measured no effect of removing the carboxyl side chain of Glu^{95} of the central pathway on the *Pf*% of the hP2X4R-E95C mutant (Fig. S6 *D* and *E*), despite the fact that this site forms a cation-binding site in the zfP2X4.1R (8).

Our finding that removing the fixed negative charge of Glu^{56} has no effect on *Pf*% is interesting in light of the opposite effects of MTSET$^+$ and MTSES$^-$ on the single channel conductance of the E56C mutant (Fig. 4). Glu^{56} is on the outer rim of the lateral portal where the negative charge of the native carboxylate may be poorly positioned to alter current (Fig. S3). In contrast, the addition of the bulky (≈6 Å) anionic headgroup of MTSES$^-$ to the cysteine mutant may place fixed negative charge closer to the path of ion flow and, thus, increase single channel current by attracting cations to the lateral portals.

Central Vestibule. We then extended our cysteine scan to determine the accessibility of four sites (Ser^{59}, Val^{61}, Ser^{62}, Asn^{97}) in the central vestibule to a range of MTS reagents (Fig. S3). Our rationale for doing this experiment was as follows: The central vestibule sits just above the lateral portals, and although most cations that exit the

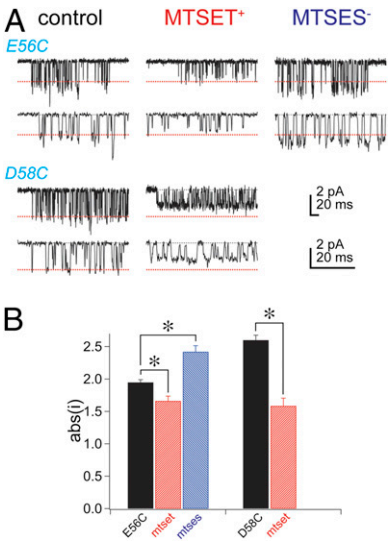

Fig. 4. Thiolation alters in single channel current. (*A*) Representative single-channel currents of unmodified E56C and D58C receptors are shown at two different time scales (*Left*). *Center* shows the reduction of current through E56C and D58C in cells bathed in 1 mM MTSET$^+$ before patch formation. *Right* shows the increase in current amplitude in a cell expressing the E56C mutant and exposed to 1 mM MTSES$^-$. The dashed red lines indicate the average single-channel current amplitude of the relevant unmodified mutant receptors. (*B*) The histogram presents the average of all of the data shown in Fig. S5C. Asterisks denote significant differences ($P < 0.01$) in current amplitudes for the E56C and D58C mutants measured before and after thiolation.

portals probably move passively down the transmembrane electrochemical gradient and into the cell, some may be attracted to the strong electronegative pull of acidic amino acids in the central vestibule (8, 9). In keeping with this hypothesis, we found that $MTSET^+$ significantly potentiated the ATP-gated currents of S59C, S62C, and N97C mutants (Fig. S7). In contrast, $MTSES^-$ potentiated the current of the receptors carrying the S59C mutation that sits just above the lateral portals, but neither altered ATP-gated current nor masked the effects of $MTSET^+$ on S62C and N97C. Neither $MTSET^+$ nor $MTSES^-$ affected V61C. Thus, our results support the hypothesis of Kawate et al. that the negative electrostatic environment of the central vestibule attracts cations and repels cations (8). The head groups of $MTSET^+$ and $MTSES^-$ are approximately the same size (14), which suggests that the lack of effect of $MTSES^-$ on S62C and N97C cannot be explained by bulk exclusion. Rather, the data imply that the strong electronegative environment of the central cavity impedes the flow of anions through the middle third of the central pathway, despite the fact that $MTSES^-$ readily modifies downstream engineered cysteines in the lateral portals (E56C, D58C) and transmembrane pore (S341C).

Effect of Ivermectin on Thiolation. Ivermectin (IVM) increases single channel conductance and lengthens mean open time of P2X4 receptors (7, 24, 26), at least in part through intercalation with the transmembrane helices (27). To determine whether the lateral portals lie in the allosteric pathway, we assessed the effects of $MTSET^+$ on the E56C and D58C mutants before and after 5-min preincubations in 1–10 μM IVM (Fig. 5*A*). IVM changed the effect of $MTSET^+$ in two ways. First, the rates of reaction were significantly slower (K_{on} values after 10 μM IVM were 1,780 ± 387 (n = 5) and 1,084 ± 200 (n = 8) for E56C and D58C, respectively). Second, the inhibitions by $MTSET^+$ were significantly smaller (Fig. 5*B*). These findings are supported by experiments using the smaller Cd^{2+} as modifier. We found that Cd^{2+} caused a pronounced potentiation and inhibition of the ATP-gated currents of the E56C and D58C mutants, respectively, and that both effects of Cd^{2+} were absent after incubation with IVM (Fig. 5 *C*–*E*). We interpret the data with $MTSET^+$ and Cd^{2+} to indicate that IVM changed the shape of the portals through an allosteric mechanism and, hence, the nature of the thiol modification.

Discussion

The main findings of this study are that cations gain access to the ion selective transmembrane pore via the lateral portals of P2X receptors and that ion flow through the portals is allosterically regulated.

The coordination of Gd^{3+} by Glu^{98} in the closed state structure of the zfP2X4.1 was interpreted to suggest that the central pathway might be a conduit for cation flow (8). However, Glu^{98} is not well conserved, and the surmountable nature of the block of ATP-evoked currents by Gd^{3+} is inconsistent with pore block (8). In relation to these facts, we found no evidence using substituted cysteine mutagenesis or measurements of *Pf%* to suggest that the central pathway is a conductive entrance to the pore.

However, our experiments provide strong evidence to suggest that ions preferentially flow to the pore via the symmetrically placed lateral portals. Thus, coapplication of ATP and either $MTSET^+$ or $MTSES^-$ causes a near complete block of current through the D58C mutant (Fig. 3*C* and Fig. S4*B*), showing that, at least under these circumstances, all or almost all of the current that enters the transmembrane pore passes first through the lateral portals. Further, $MTSES^-$ is excluded from parts of the central pathway (Fig. S7) but is still capable of modifying S341C in the transmembrane pore (Fig. S2*D*). In some ways the use of lateral portals makes intuitive sense, because some ions that traverse the central pathway might exit the pore through the three wide lateral portals rather than proceed into the single transmembrane pore. Further, the portals are short and unobstructed. The use of lateral portals therefore appears to be an efficient mechanism to facilitate unimpeded ion flow as it splits the task threefold between portals, exploits the favorable electrostatic environment near the plasma membrane outer leaflet, and reduces the diffusive path for cations.

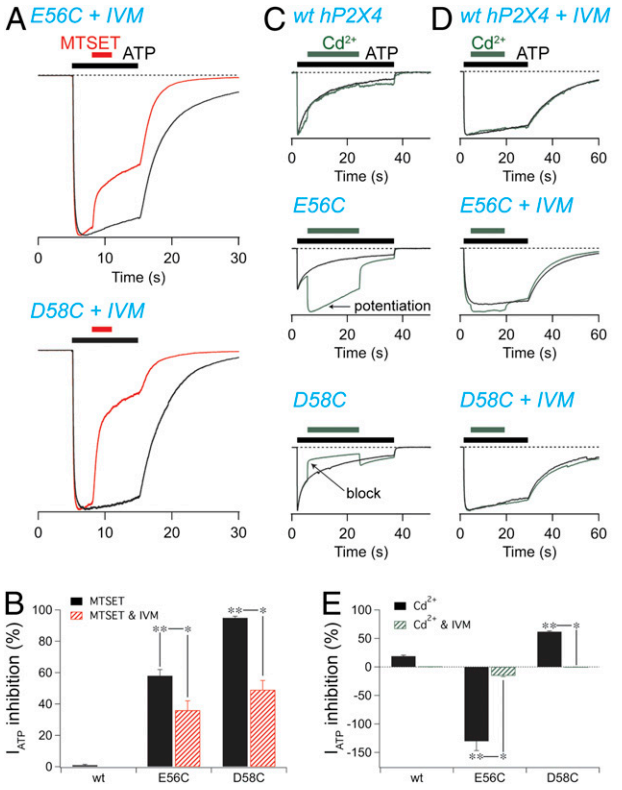

Fig. 5. IVM reduces $MTSET^+$ and Cd^{2+} modification of the lateral portals. (*A*) The figure shows the ATP-gated current before (black traces) and during (red traces) coapplication of 1 mM $MTSET^+$ in two cells preincubated in 10 μM IVM for 5 min, and then maintained in IVM for the duration of the experiment (≈10 min). The traces are normalized to their peak current amplitudes. $MTSET^+$ still blocks the ATP-gated current in cells expressing E56C and D58C and soaked in IVM, but the effect is smaller and slower. (*B*) Summary data for the block of $MTSET^+$ in the absence (black) and presence (red striped) of IVM. **, significantly different from *wt* hP2X4; *, significantly different from the *wt* and the –IVM condition ($P < 0.001$). (*C*) Normalized traces show control (black; 100 μM ATP alone) and test traces (green; 100 μM ATP followed by 20 μM Cd^{2+} applied for the duration indicated by the green bar) for *wt* hP2X4 and the indicated cysteine mutants. Arrows point to profound potentiation and block of E56C and D58C mutants by Cd^{2+}. (*D*) As in *C*, but for cells that had been bathed in 1 μM IVM for 2–5 min before the start of the recording and then also for the duration of the recording. (*E*) Summary data for experiments such as those in *C* and *D* for *wt* hP2X4R and E56C and D58C mutants. Relative to the *wt* hP2X4R, Cd^{2+} applications to E56C and D568C mutants significantly potentiated and reduced ATP-evoked responses; further these effects were abolished in the presence of IVM. The data are shown as average ± SEM (n = 5–16). **, significantly different from *wt* hP2X4R; *, significantly different from the –IVM condition.

Our finding that $MTSET^+$ reduces both whole-cell and single-channel current of the D58C mutant suggests this modification exerts a "bulk" effect in the portals that impedes the flow of ions. Cationic thiolation of D58C results in a significant (40%) reduction in single channel current that is smaller than the block of the whole-cell current (95%). The inability of thiolation to completely block single channel current by adding bulk to portal-lining residues is not surprising for two reasons. First, the lateral portals are unusually wide by comparison with the pore-lining transmembrane domains that are typical targets of thiolation studies of ion permeation (8). Second, each portal presents a single D58C side chain for modification, unlike transmembrane pores that show multiple axes of symmetry. Thus, the addition of the headgroup of $MTSET^+$ to a single cysteinyl side chain in a wide lateral portal may not fully plug the opening. If so, then the almost complete reduction in whole-cell current by $MTSET^+$ must reflect changes in both conduction and gating. A change in gating after thiolation

is more often the rule than the exception (14). Nevertheless, our finding that $MTSET^+$ (and $MTSES^-$) change the amplitudes of the single channel currents of E56C and D58C provides unusually strong support for the hypothesis that the lateral portals form a primary entrance to the transmembrane ion conduction pathway.

A dual effect on conduction and gating may also explain the smaller effect of $MTSET^+$ on homologous residues of the rP2X2R. The effect of $MTSET^+$ on the ATP-gated current of rP2X2R-D57C and rP2X2R-E59C is smaller (28) than the effect on the homologous residues (E56C, D58C) of hP2X4R, which could be explained if some of the effect of thiolation results from a change in gating, as discussed above. In fact, the gating behavior of rP2X2R and hP2X4R differ in sensitivity to agonists, antagonists, and allosteric modulators like pH and IVM (29). Perhaps then we should not be surprised that the effect of thiolation also differs between P2X receptors. Nevertheless, the route of access is the main consideration, and our data clearly show that MTS reagents alter ATP-gated current of the hP2X4R by entering the lateral portals.

Some of the accessible residues (Ser^{59}, Ser^{62}, Asn^{97}) that are potentiated by thiolation map to a region between the proposed ATP binding site and the outer end of TM1, composed of "connecting rods" that link ATP binding to movement of the transmembrane domains (30). Residues in this part of the protein are thought to be involved in gating (30, 31). Our results suggest that the connecting rods form a surface of the portals and vestibules that is accessible to application of water-soluble thiol-reactive reagents that travel through the lateral portals even when the transmembrane channel gate is closed. Further, our data with IVM, a known allosteric regulator of P2X4 receptors, provides good evidence that altered gating can affect the nature of accessibility in the portals. This observation, along with the connecting rods model, implies that ion flow through the lateral portals and receptor gating may be linked. These findings raise the possibility that ion access to the hP2X4R portals could be targeted with designer drugs, which may find applications in therapy of P2X4-associated disorders. In future work it will be useful to explore this possibility when a 3D structure of the open channel bound to ATP becomes available.

In conclusion, our experiments show a pattern of hits in cysteine scanning accessibility experiments (Fig. S8) that strongly suggest that ions access the pore of a P2X receptor by making preferential use of three radially symmetric and unobstructed lateral portals. Although we found no evidence to support current flow through the central pathway, it is still a possibility that this route is used under conditions that differ from those used in our experiments, for example, when the concentration of extracellular divalents is lowered to promote pore dilation (1). Finally, our findings are directly relevant to trimeric acid sensing channels (9, 10) and to structural and mechanistic studies of other membrane proteins containing portals (32, 33), which may also be regulated and used by the transported species.

Methods

Methods are fully described in *SI Methods*. In short, whole-cell and single-channel currents were recorded from cultured HEK293 cells that transiently expressed either *wt* or cysteine-substituted hP2X4Rs. Broken-patch voltage-clamp was used to record whole-cell current when one or two applications of ATP were sufficient to compete the goals the experiment. To prevent run-down with repeated drug applications, the perforated-patch voltage clamp was used to record whole-cell current when more than two applications were required. Thiol modification was determined from changes in ATP-gated (100 μM) current measured before, during, and after applications of MTS (1 mM) or Cd^{2+} (20 μM). Single-channel current was recorded from cell-attached patches of cells whose membrane potential was zeroed by a bath solution containing 154 mM K^+. The transmembrane potential was set to −120 mV by applying current to the recording electrode. Recording electrodes were filled with a solution containing 140 mM NaF and 0.1–1.0 μM ATP. *Pf*% was measured as described (20, 24).

ACKNOWLEDGMENTS. We thank Dr. Florentina Soto for the gift of the hP2X4 plasmid; Kelsey Eckelkamp for help with cell biology and tissue culture; and Dr. Decha Enkvetchakul for comments on an earlier version of the manuscript. This work was supported by National Institute of Health Grants HL56236 and NS063186.

1. North RA (2002) Molecular physiology of P2X receptors. *Physiol Rev* 82:1013–1067.
2. Surprenant A, North RA (2008) Signaling at purinergic P2X receptors. *Annu Rev Physiol* 71:333–359.
3. Khakh BS, North RA (2006) P2X receptors as cell-surface ATP sensors in health and disease. *Nature* 442:527–532.
4. Torres GE, Egan TM, Voigt MM (1999) Hetero-oligomeric assembly of P2X receptor subunits. Specificities exist with regard to possible partners. *J Biol Chem* 274:6653–6659.
5. Nörenberg W, Illes P (2000) Neuronal P2X receptors: Localisation and functional properties. *Naunyn Schmiedebergs Arch Pharmacol* 362:324–339.
6. Jarvis MF (2010) The neural-glial purinergic receptor ensemble in chronic pain states. *Trends Neurosci* 33:48–57.
7. Stojilkovic SS, Yan Z, Obsil T, Zemkova H (2010) Structural insights into the function of P2X4: An ATP-gated cation channel of neuroendocrine cells. *Cell Mol Neurobiol* 30:1251–1258.
8. Kawate T, Michel JC, Birdsong WT, Gouaux E (2009) Crystal structure of the ATP-gated P2X(4) ion channel in the closed state. *Nature* 460:592–598.
9. Gonzales EB, Kawate T, Gouaux E (2009) Pore architecture and ion sites in acid-sensing ion channels and P2X receptors. *Nature* 460:599–604.
10. Jasti J, Furukawa H, Gonzales EB, Gouaux E (2007) Structure of acid-sensing ion channel 1 at 1.9 A resolution and low pH. *Nature* 449:316–323.
11. Rassendren F, Buell G, Newbolt A, North RA, Surprenant A (1997) Identification of amino acid residues contributing to the pore of a P2X receptor. *EMBO J* 16:3446–3454.
12. Egan TM, Haines WR, Voigt MM (1998) A domain contributing to the ion channel of ATP-gated P2X2 receptors identified by the substituted cysteine accessibility method. *J Neurosci* 18:2350–2359.
13. Kawate T, Robertson JL, Li M, Silberberg SD, Swartz KJ (2011) Ion access pathway to the transmembrane pore in P2X receptor channels. *J Gen Physiol* 137:579–590.
14. Karlin A, Akabas MH (1998) Substituted-cysteine accessibility method. *Methods Enzymol* 293:123–145.
15. Schneggenburger R, Zhou Z, Konnerth A, Neher E (1993) Fractional contribution of calcium to the cation current through glutamate receptor channels. *Neuron* 11:133–143.
16. Vernino S, Rogers M, Radcliffe KA, Dani JA (1994) Quantitative measurement of calcium flux through muscle and neuronal nicotinic acetylcholine receptors. *J Neurosci* 14:5514–5524.
17. Diaz-Hernandez M, et al. (2002) Cloning and characterization of two novel zebrafish P2X receptor subunits. *Biochem Biophys Res Commun* 295:849–853.
18. Li M, Chang TH, Silberberg SD, Swartz KJ (2008) Gating the pore of P2X receptor channels. *Nat Neurosci* 11:883–887.
19. Kracun S, Chaptal V, Abramson J, Khakh BS (2010) Gated access to the pore of a P2X receptor: Structural implications for closed-open transitions. *J Biol Chem* 285:10110–10121.
20. Roberts JA, et al. (2008) Cysteine substitution mutagenesis and the effects of methanethiosulfonate reagents at P2X2 and P2X4 receptors support a core common mode of ATP action at P2X receptors. *J Biol Chem* 283:20126–20136.
21. Samways DS, Egan TM (2007) Acidic amino acids impart enhanced Ca2+ permeability and flux in two members of the ATP-gated P2X receptor family. *J Gen Physiol* 129:245–256.
22. Kronengold J, Trexler EB, Bukauskas FF, Bargiello TA, Verselis VK (2003) Single-channel SCAM identifies pore-lining residues in the first extracellular loop and first transmembrane domains of Cx46 hemichannels. *J Gen Physiol* 122:389–405.
23. Johnson JP, Jr., Zagotta WN (2005) The carboxyl-terminal region of cyclic nucleotide-modulated channels is a gating ring, not a permeation path. *Proc Natl Acad Sci USA* 102:2742–2747.
24. Priel A, Silberberg SD (2004) Mechanism of ivermectin facilitation of human P2X4 receptor channels. *J Gen Physiol* 123:281–293.
25. Egan TM, Khakh BS (2004) Contribution of calcium ions to P2X channel responses. *J Neurosci* 24:3413–3420.
26. Khakh BS, Proctor WR, Dunwiddie TV, Labarca C, Lester HA (1999) Allosteric control of gating and kinetics at P2X(4) receptor channels. *J Neurosci* 19:7289–7299.
27. Silberberg SD, Li M, Swartz KJ (2007) Ivermectin Interaction with transmembrane helices reveals widespread rearrangements during opening of P2X receptor channels. *Neuron* 54:263–274.
28. Jiang LH, Rassendren F, Surprenant A, North RA (2000) Identification of amino acid residues contributing to the ATP-binding site of a purinergic P2X receptor. *J Biol Chem* 275:34190–34196.
29. Jarvis MF, Khakh BS (2009) ATP-gated P2X cation-channels. *Neuropharmacology* 56:208–215.
30. Browne LE, Jiang LH, North RA (2010) New structure enlivens interest in P2X receptors. *Trends Pharmacol Sci* 31:229–237.
31. Jiang R, et al. (2010) A putative extracellular salt bridge at the subunit interface contributes to the ion channel function of the ATP-gated P2X2 receptor. *J Biol Chem* 285:15805–15815.
32. Peters JA, et al. (2010) Novel structural determinants of single channel conductance and ion selectivity in 5-hydroxytryptamine type 3 and nicotinic acetylcholine receptors. *J Physiol* 588:587–596.
33. Unwin N (2005) Refined structure of the nicotinic acetylcholine receptor at 4A resolution. *J Mol Biol* 346:967–989.

Supporting Information

Samways et al. 10.1073/pnas.1017550108

SI Methods

Homology Modeling. Human and zebrafish P2X4 sequences have 57.5% identity and 74.9% similarity, and we therefore used the crystal structures of the zfP2X.1R (1) as templates to build a hP2X4R model. First, the highest resolution structure of zfP2X4.1R (PDB ID code 3H9V), which contained only one monomer, was used to create a 3D model of a hP2X4R monomer by using the homology modeling server SWISSMODEL (2). In a second step, the lower resolution structure of the full zfP2X4.1R trimer (PDB ID code 3I5D) was used to direct the symmetry of three hP2X4R monomers, which constituted the complete model. Finally, the hP2X4R model was minimized by using the GROMOS force-field implemented in the program DEEP VIEW (3). The root mean square deviation between single chains of the hP2X4 model and zfP2X4.1 structure is 0.11 Å (alignment of 329 atoms), demonstrating a good fit of the model to the structure. Because zfP2X4.1R was solved as a truncated receptor missing both the N- and C- intracellular domains, these domains are absent in our homology model of the hP2X4R. At present, data do not support a role for these domains in forming the ion channel pore.

The central ion pathway was calculated by using PORE WALKER 1.0 (4). CAVER 2.0 v0.003 (5) was used to map the alternative ion pathway through the lateral portals. The starting point for calculation was defined as the resulting coordinates of Ser^{341} from each subunit. The results are displayed by using PyMol 1.3 (Schrödinger, LLC).

Cell Culture and Molecular Biology. HEK293 cells were maintained in exponential growth in DMEM supplemented with 10% heat-inactivated FBS, 2 mM glutamine, 50 units/mL penicillin G, and 50 μg/mL streptomycin (all reagents from Invitrogen) and incubated at 37 °C in a humidified atmosphere with 5% CO_2. Upon reaching 70–80% confluency in 75-cm^2 tissue culture flasks, the cells were enzymatically dissociated, and transfected with a P2X plasmid and a fluorescent reporter gene by using Lipofectamine LTX (Invitrogen). The cells were replated in 35-mm culture dishes and left to grow for 48 h before use in experiments. Mutagenesis was accomplished by using the QuikChange Lightning Site-Directed Mutagenesis kit (Agilent Technologies) and verified by automated DNA sequencing (Retrogen).

Whole-Cell Electrophysiology. We used standard broken-patch whole-cell recording technique when one or two ATP applications were needed to complete an experiment (see, for example, Fig. 2 *B* and *D*), and we used the perforated-patch method when >2 drug applications were needed (see, for example, Fig. 2 *C* and *E*). The broken-patch method is quicker and more efficient that the perforated-patch method, but complicated by a progressive loss of peak current amplitude in response to repeated applications of ATP. In contrast, we saw reproducible responses to ATP when using the perforated-patch method, as reported for the rat P2X1 receptor (6). On the morning of an experiment, transfected cells on 35-mm plates were dissociated by using a Trypsin/EDTA solution (Invitrogen), and then replated at low density for 2 h before experiments began. Then, the cells were again dispersed by mechanical agitation of the culture media, and an aliquot of dispersed cells was transferred to a recording chamber mounted an inverted fluorescence microscope. Current was recorded from single cells by using Axon 200b amplifiers (Mechanical Devices), ITC-16 D/A boards (Heka Instruments), and AxoGraphX Software (AxoGraph). Current was low pass filtered at 1 kHz, sampled at a rate of 10 kHz, and stored on magnetic drives for off-line analyses. Drugs were applied by using the Perfusion Fast-Step SF-77 System (Warner Instruments). For a more complete description of our perforated-patch methods, see Migita et al. (7) and Li et al. (8). For a complete description of the broken-patch method and our protocol to measure the effects of Cd^{2+} on P2X receptors, see Kracun et al. (9).

Single-Channel Electrophysiology. Cells were maintained and dispersed as described above. Single-channel current was recorded from cell-attached patches from dispersed cells by using fire-polished 7052 glass electrodes (Garner Glass Company) with open tip resistances of 5–12 MΩ. These electrodes were coated at their tips with HIPEC R6101 semiconductor protective coating (Dow Corning) and filled with a solution of the following composition: 0.0003–0.001 mM ATP, 140 mM NaF, 5 mM NaCl, 10 mM Hepes, 1 mM $CaCl_2$ at pH 7.3 with NaOH. We used a high K^+ solution of the following composition to set the transmembrane potential of the whole cell close to 0 mV: 154 mM KCl, 1 mM $CaCl_2$, 1 mM $MgCl_2$, 10 mM glucose, 10 mM Hepes at pH 7.4 with KOH. After formation of the gigaseal (>10 GΩ), current was low-pass filtered at 5 kHz, digitized direct to the computer hard drive at a sampling rate of 50 kHz, and subsequently analyzed off-line by using IGOR Pro (Wavemetrics). The currents shown in Fig. 4 and Fig. S5 were furthered filtered at 2 kHz using the low-pass software filter of AxoGraphX for display only. Single-channel current amplitude was estimated from the best Gaussian fit to an all-points amplitude histogram of a leak-subtracted trace of a single burst of ATP-gated channel activity, using IGOR Pro.

Statistical Analyses. All data are presented as the mean ± SEM. Drug treatments were analyzed by comparing data obtained before, during, and after drug treatment by using the Student *t* test function. Groups of data were analyzed by one-way ANOVA with significance determined from the Tukey's protected multiple comparison test using Instat (GraphPad Software). A $P \leq 0.01$ was considered significant.

Patch Clamp Photometry. *Pf*% was determined by using the dye-overload method of Neher (10) and Dani (11) as described in detail in published papers from our laboratory (12, 13). ATP-gated whole-cell current was recorded from adherent HEK293 cells by using a recording pipette containing 140 mM CsCl, 10 mM tetraethylammonium, 3 mM CsOH, 10 mM Hepes, and 2 mM K_5-fura-2. These cells were perfused with an extracellular buffer containing 140 mM NaCl, 2 mM $CaCl_2$, 1 mM $MgCl_2$, 3 mM NaOH (pH 7.4), 10 mM glucose, and 10 mM Hepes. Fura-2 fluorescence was measured with a Model 714 Photomultiplier Detection System (Photon Technology International). *Pf*% was determined from the following equation:

$$Pf\% = \frac{\Delta F_{380}/F_{\max}}{Q_T} \times 100,$$

where ΔF_{380} is the change in fura-2 fluorescence caused by Ca^{2+} entry, Q_T is the leak-subtracted integrated current recorded using patch clamp electrophysiology, and F_{max} is a proportionality constant determined as described (12).

Effects of Thiol-Reactive Reagents. Thiol modification was determined from changes in ATP-gated current measured before, during, and after applications of MTS or Cd^{2+}. In all cases, we used

a saturating concentration of ATP (100 μM) to fully activate the receptor, and at least 3 min passed between applications to minimize rundown. For modification in the absence of ATP (i.e., closed state modification), we measured the membrane current elicited by short (1 s) applications of ATP (100 μM) applied before and after a 2- to 60-s application of 1 mM MTS alone by using the perforated-patch technique of whole-cell voltage clamp. Percent change was determined from the average of the peak current amplitudes of five applications of ATP administered before and after MTS. For modification during channel gating (open state modification), we initiated an agonist response by applying 100 μM ATP, and then switched to a solution containing ATP and either MTS (1 mM for 3 s) or Cd^{2+} (20 μM for 15 s). In this case, we recorded current by using the whole-cell voltage-clamp technique because it is more expeditious than the perforated-patch method. (In control experiments, we found no difference between methods in the effect of thiol-reactive reagents on agonist-gated current when coapplied with ATP). Then, the percent change was determined by dividing the agonist-gated current amplitude measured just before application of MTS or Cd^{2+}, by the agonist-gated current amplitude measured at the end of the rapid (usually <1 s) exponential fade in current caused by the thiol modifier.

We assume that the reaction of MTS with the thiol side chain of cysteine is irreversible. If so, then the apparent rate of modification rate (K_{on}) is equal to:

$$K_{\text{on}} = \frac{1}{\tau_{on} \times [MTS]},$$

where τ_{on} is the time constant of modification measured from the single exponential fit of the immediate change in agonist-gated current that occurs upon introduction of an MTS reagent.

Pharmacology. In each cell, ATP-gated current was normalized by dividing its peak amplitude by the average of the peak amplitudes of two or more previous applications of 30 μM ATP, as described (8). Concentration–response curves for individual cells were then fit with the Hill equation by using the Levenberg–Marquardt algorithm implemented in IGOR Pro (Wavemetrics):

$$Y = \frac{Y_{\max}}{1 + (\text{EC}_{50}/X)^{\text{nH}}},$$

where Y is the current amplitude, and X is the concentration of ATP. The fit was used to estimate the maximum response ($Y_{\max}$), the concentration of ATP needed to generate the half-maximal response (EC_{50}), and the Hill slope (nH). Current amplitudes after $MTSET^{+}$ were normalized to control responses to 30 μM ATP measured before thiol modification.

1. Kawate T, Michel JC, Birdsong WT, Gouaux E (2009) Crystal structure of the ATP-gated P2X(4) ion channel in the closed state. *Nature* 460:592–598.
2. Schwede T, Kopp J, Guex N, Peitsch MC (2003) SWISS-MODEL: An automated protein homology-modeling server. *Nucleic Acids Res* 31:3381–3385.
3. Guex N, Peitsch MC (1997) SWISS-MODEL and the Swiss-PdbViewer: An environment for comparative protein modeling. *Electrophoresis* 18:2714–2723.
4. Pellegrini-Calace M, Maiwald T, Thornton JM (2009) PoreWalker: A novel tool for the identification and characterization of channels in transmembrane proteins from their three-dimensional structure. *PLOS Comput Biol* 5:e1000440.
5. Petrek M, et al. (2006) CAVER: A new tool to explore routes from protein clefts, pockets and cavities. *BMC Bioinformatics* 7:316.
6. Lewis CJ, Evans RJ (2000) Lack of run-down of smooth muscle P2X receptor currents recorded with the amphotericin permeabilized patch technique, physiological and pharmacological characterization of the properties of mesenteric artery P2X receptor ion channels. *Br J Pharmacol* 131:1659–1666.
7. Migita K, Haines WR, Voigt MM, Egan TM (2001) Polar residues of the second transmembrane domain influence cation permeability of the ATP-gated P2X(2) receptor. *J Biol Chem* 276:30934–30941.
8. Li Z, Migita K, Samways DS, Voigt MM, Egan TM (2004) Gain and loss of channel function by alanine substitutions in the transmembrane segments of the rat ATP-gated P2X2 receptor. *J Neurosci* 24:7378–7386.
9. Kracun S, Chaptal V, Abramson J, Khakh BS (2010) Gated access to the pore of a P2X receptor: Structural implications for closed-open transitions. *J Biol Chem* 285:10110–10121.
10. Schneggenburger R, Zhou Z, Konnerth A, Neher E (1993) Fractional contribution of calcium to the cation current through glutamate receptor channels. *Neuron* 11:133–143.
11. Vernino S, Rogers M, Radcliffe KA, Dani JA (1994) Quantitative measurement of calcium flux through muscle and neuronal nicotinic acetylcholine receptors. *J Neurosci* 14: 5514–5524.
12. Egan TM, Khakh BS (2004) Contribution of calcium ions to P2X channel responses. *J Neurosci* 24:3413–3420.
13. Samways DS, Egan TM (2007) Acidic amino acids impart enhanced Ca2+ permeability and flux in two members of the ATP-gated P2X receptor family. *J Gen Physiol* 129: 245–256.
14. Priel A, Silberberg SD (2004) Mechanism of ivermectin facilitation of human P2X4 receptor channels. *J Gen Physiol* 123:281–293.

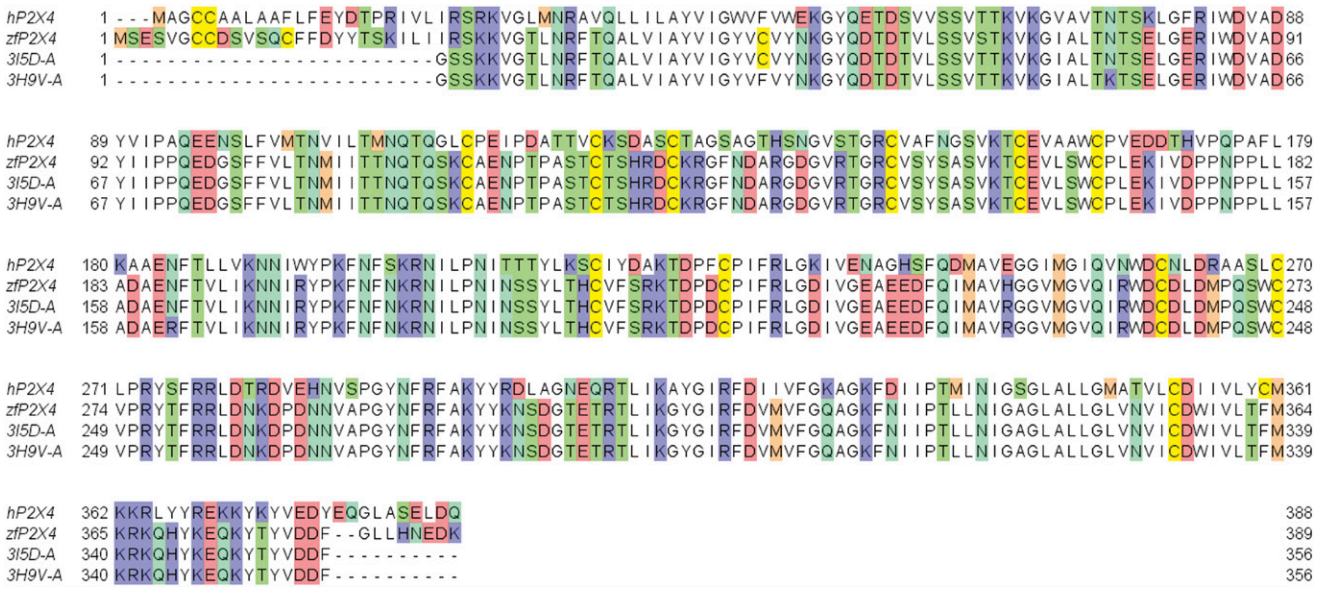

Fig. S1. Sequence alignment of hP2X4R and zfP2X4R4.1 with the truncated 315D-A and 3H9V-A structures of Kawate et al (1).

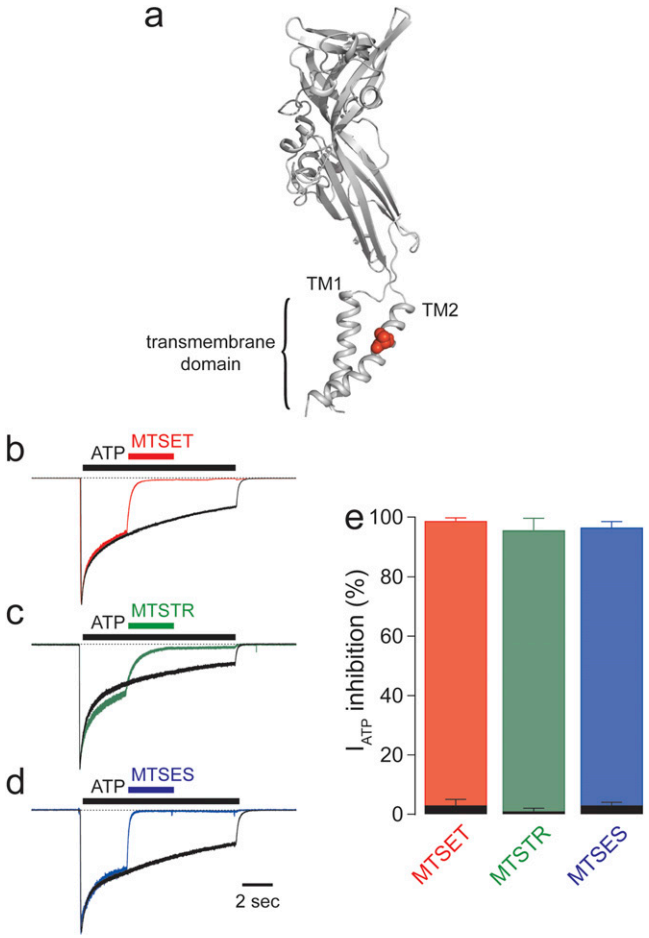

Fig. S2. The effect of three MTS reagents on the transmembrane hP2X4R-S341C mutant. (*A*) The transmembrane position of Ser^{341} in shown in a single subunit of trimeric hP2X4R. ATP current through hP2X4R-S341C was irreversibly inhibited by $MTSET^{+}$ (*B*), MTSTR (*C*), and $MTSES^{-}$ (*D*). In each case, the traces are normalized to peak currents. (*E*) Average data of five or more cells. The black bars represent the average response of *wt* hP2X4R to each MTS reagent.

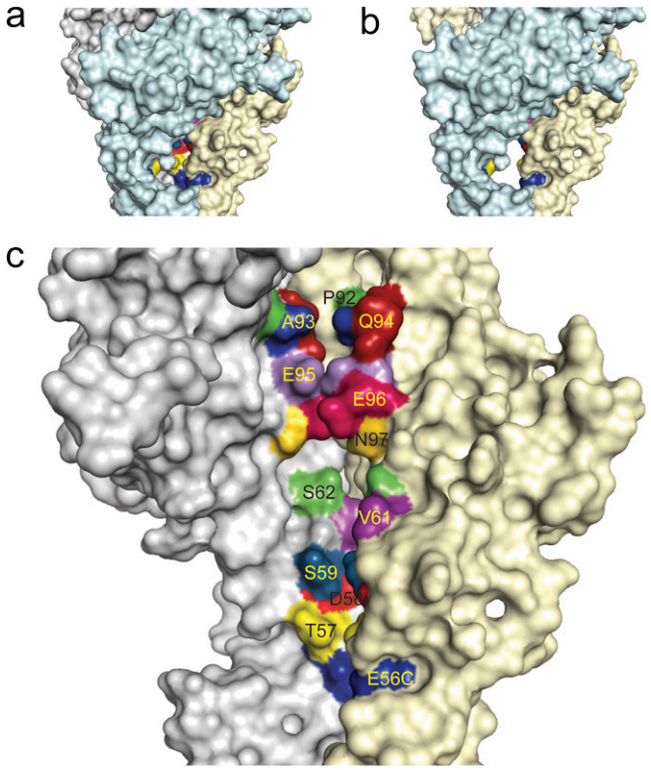

Fig. S3. Surface representation of hP2X4R showing residues in the lateral portals, extracellular vestibule, and central vestibule. (*A*) All three subunits of the trimeric protein at the level of the lateral portals. (*B*) The subunit at the back of the protein is removed to clearly show a portal entrance formed by adjoining subunits. (*C*) The front subunit is removed to show positions of residues tested in this study.

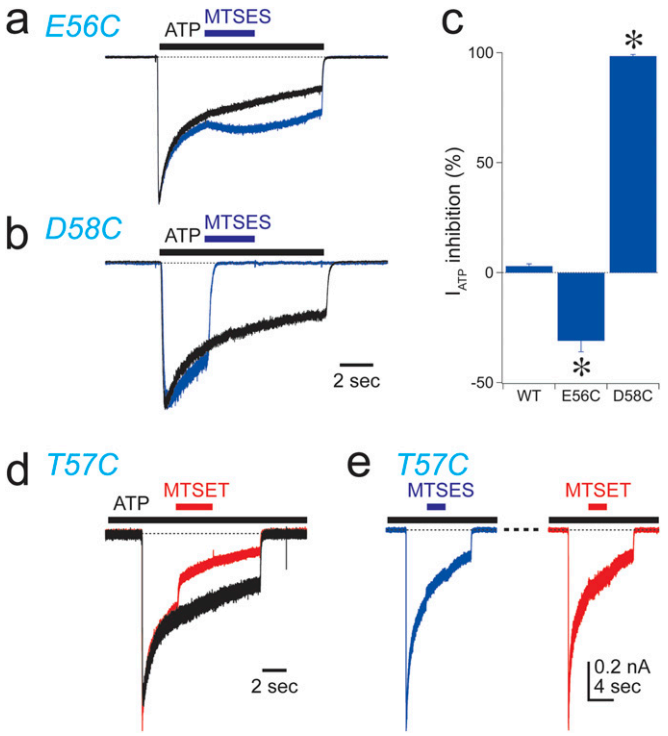

Fig. S4. The effects of $MTSES^-$ on E56C, T57C, and D58C. (*A*) $MTSES^-$ (1 mM) caused a slow (K_{on} = 847 ± 109, n = 9) potentiation of current through E56C. Black trace is control, and blue trace is a recording showing the effect of coapplication of $MTSES^-$. (*B*) $MTSES^-$ (1 mM) caused a near complete block of current through D58C mutants. (*C*) Averaged data for $MTSES^-$. The asterisks indicate significant differences from the wt hP2X4R ($P < 0.001$). $MTSES^-$ had no significant effect on the *wt* hP2X4R (n = 5). (*D*) $MTSET^+$ blocks the ATP-gated current of the T57C mutant. Black trace is control, and red trace is a recording showing the effect of coapplication of $MTSET^+$. (*E*) Shown are two traces, separated by a 10-min wash. First, $MTSES^-$ was coapplied with ATP (blue trace). This was then followed by coapplication of $MTSET^+$ and ATP. Previous exposure to $MTSES^-$ blocked the inhibitory effect of $MTSET^+$ (see *D*) on the ATP-gated current.

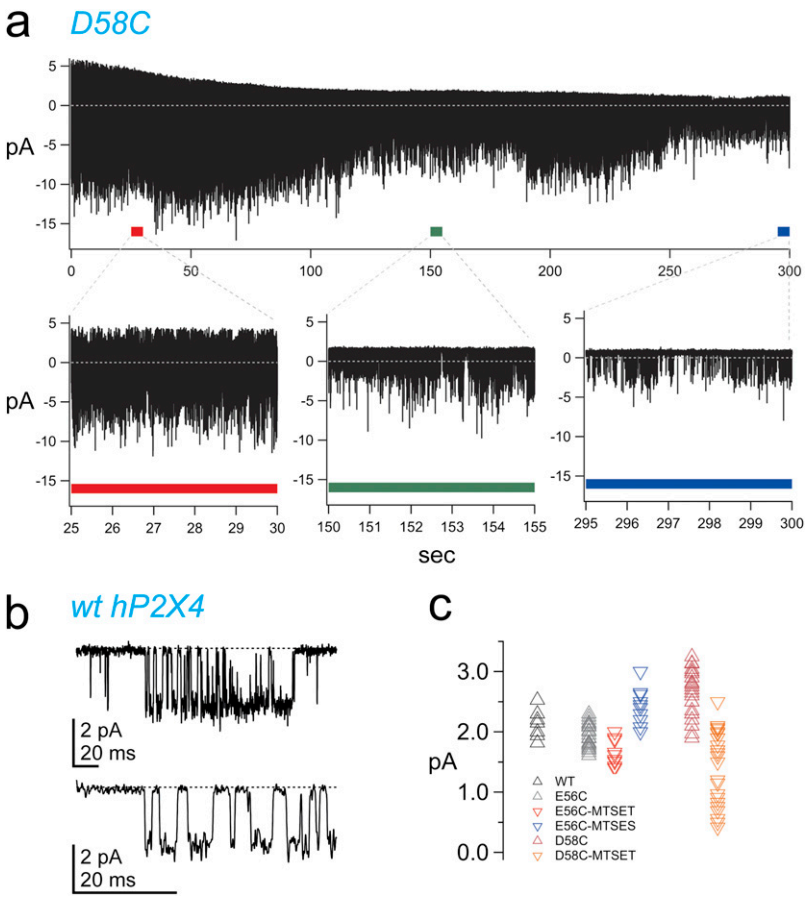

Fig. S5. (*A*) The traces show the single channel activity of a cell-attached patch from a HEK293 cell expressing hP2X4R-D58C. The transmembrane potential was −120 mV, and the recording electrode contained a NaF solution and 1 μM ATP. See *SI Methods* for a complete description of the protocol. The recording began ≈20 s after formation of the gigaseal. The patch contained at least four receptors whose activity gradually decreased over time. The three lower panels show 5 s segments of the upper trace on an expanded time scale. (*B*) Single-channel current of the *wt* hP2X4R shown at two different time scales. We found that the hP2X4R opened in bursts of channel activity as described (14). (*C*) Scatter plot of the single-channel current amplitudes of all data used to construct the bar graph of Fig. 4*B*. ATP-gated channels were identified as bursts of openings that were unlikely any seen in the absence of ATP. The data of each column shows a normal distribution.

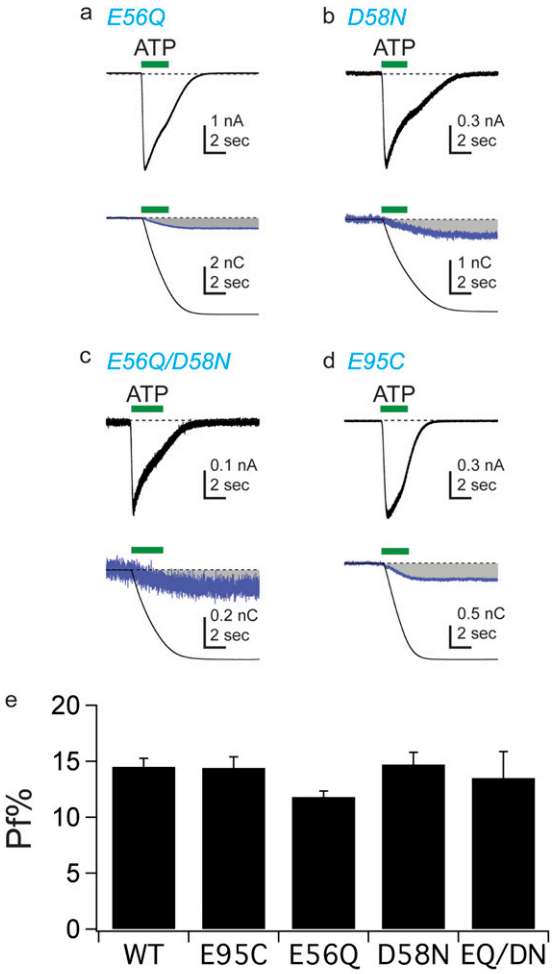

Fig. S6. *Pf*% is unchanged in hP2X4R mutants. Representative current and fluorescence recordings for portal mutants hP2X4R-E56C (*A*), hP2X4R-D58C (*B*), and hP2X4RE56C/D58C (*C*) expressed in HEK293 cells. ATP (30 μM) was applied for 2 s. In each case, *Upper* shows the ATP-gated current, and *Lower* shows the charge carried by Ca^{2+} (i.e., Q_{Ca}, blue traces, determined from fluorescence; see *SI Methods*) relative (shaded area) to the total ATP-gated charge (i.e., Q_T, black traces). We also measured the *Pf*% of the hP2X4R-95C mutant (*D*). We did this experiment because the homologous residue (Glu^{98}) is suggested to form a cation-binding site in the zfP2X4.1R. We saw no effect on *Pf*% of removing the carboxylate side chain. (*E*) Averaged data. In all cases, the *Pf*% values were not significantly different from that of the wild-type receptor ($P > 0.05$).

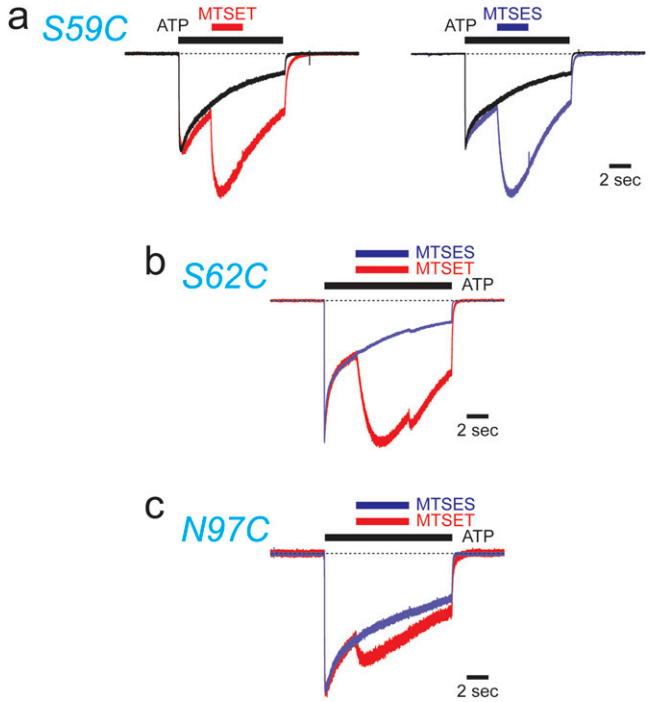

Fig. S7. The effects of $MTSET^+$ and $MTSES^-$ on S59C, S62C, and N97C in the central cavity measured by using broken-patch whole cell electrophysiology. (*A*) Both $MTSET^+$ (*Left*) and $MTSES^-$ (*Right*) potentiate the current of the S59C mutant generated by using a saturating dose (100 μM) of ATP. (*B* and *C*) In HEK293 cells expressing either the hP2X4R-S62C (*A*) or hP2X4R-N97C (*B*) mutant, application of $MTSES^-$ (1 mM) in the presence of ATP cause no change in current amplitude (blue traces). However, unlike the situation seen using the T57C mutant (Fig. S4*E*), a prior application of $MTSES^-$ does not prevent a potentiation caused by a subsequent coapplication of ATP and $MTSET^+$ (red traces). These data suggest that S62C and N97C, which are positioned in the upper part of the central vestibule (Fig. S3), are inaccessible to the anionic modifying reagent.

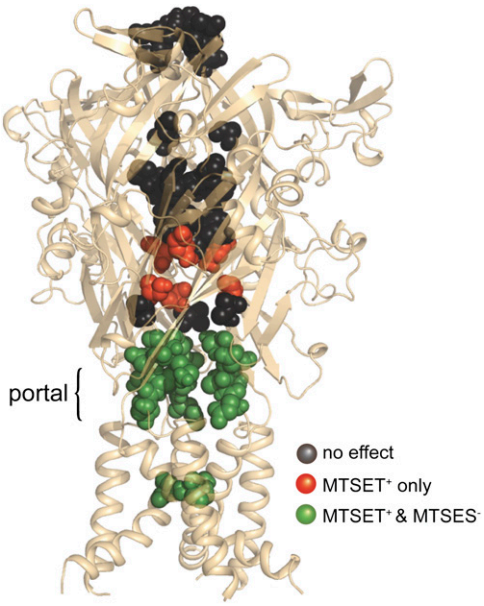

Fig. S8. Illustration of hP2X4R showing the locations of cysteine substitutions that render the mutants sensitive to modification by $MTSET^+$ alone (red) or both $MTSET^+$ and $MTSES^-$ (green). Positions carrying cysteine mutations that conferred no sensitivity are shown in black.